Type-II superlattice detector for long-wave infrared imaging

*P. C. Klipstein, E. Avnon, Y. Benny, A. Fraenkel, A. Glozman, E. Ilan, E. Kahanov, O. Klin, L. Langof, †Y. Livneh, I. Lukomsky, M. Nitzani, L. Shkedy, I. Shtrichman, N. Snapi, R. Talmor, †A. Tuito, S. Vaserman, and E. Weiss

SemiConductor Devices P.O. Box 2250, Haifa 31021, Israel

†Israel MOD

ABSTRACT

When incorporated into the active layer of a "XB*p*" detector structure, Type II InAs/GaSb superlattices (T2SLs) offer a high quantum efficiency (QE) and a low diffusion limited dark current, close to MCT Rule 07. Using a simulation tool that was developed to predict the QE as a function of the T2SL period dimensions and active layer stack thickness, we have designed and fabricated a new focal plane array (FPA) T2SL XB*p* detector. The detector goes by the name of "Pelican-D LW", and has a format of 640 × 512 pixels with a pitch of 15 μm. The FPA has a QE of 50% (one pass), a cut-off of ~9.5 μm, and operates at 77K with a high operability, background limited performance and good stability. It uses a new digital read-out integrated circuit, and the integrated detector cooler assembly (IDCA) closely follows the configuration of SCD's Pelican-D MWIR detector.

Keywords: Infrared Detector, LWIR, Focal Plane Array, Bariode, Type II superlattice, XBp, pBp

1. INTRODUCTION

High performance photodiode Focal Plane Array (FPA) detectors that operate in the Mid or Long Wave Infra-Red (MWIR or LWIR) "window" of the atmosphere are often made from Mercury Cadmium Telluride (MCT), because of the potential tunability of the band gap and the low "diffusion" limited dark current[1]. However, the need for high quality Cadmium Zinc Telluride (CZT) substrates makes them expensive and difficult to scale to large areas. Recently, the InAs/GaSb Type II superlattice (T2SL) has emerged as a serious competitor material to MCT because, like MCT, it also offers tunability over the full MWIR and LWIR ranges. Although T2SL diodes have a dark current dominated by Shockley-Read-Hall traps in the depletion region and so are generation-recombination (G-R) limited[2], the G-R problem has recently been overcome using a patented "XB*p*" barrier device technology[3,4] which can be implemented in T2SL devices grown on commercial GaSb substrates. It provides a low diffusion limited dark current as in MCT, but with many of the advantages of III-V materials, including the potential for scalability to large areas at affordable cost. In this work we introduce a new, high performance, 15 μm pitch focal plane array (FPA) detector with a 9.5 μm cut-off wavelength based on a LWIR T2SL barrier device grown lattice matched to GaSb, using Molecular Beam Epitaxy (MBE).

* *Email*: philip_k@scd.co.il

This paper is arranged as follows. In section 2, the XB*p* concept is introduced. In section 3, the implementation of the XB*p* architecture in a LWIR T2SL device is presented, and theoretical predictions are compared with experimental measurements of dark current and quantum efficiency (QE) in test devices. The next section introduces the key parameters of SCD's new 15 µm pitch, 640 × 512 read-out integrated circuit (ROIC) designed to operate with XB*p* devices (equivalent polarity to *n*-on-*p* photo-diodes). The radiometric characteristics of the new FPA are presented in section 5, and conclusions are summarized in section 6.

2. XB*p* DEVICES

Schematic band diagrams for a T2SL $XB_p p$ detector[5], are shown in Figure 1. The device contains a contact layer (CL) which can be made in several ways including from an *n*- or *p*-type InAs/GaSb T2SL (it is given the general symbol "X"), a *p*-type barrier layer (BL) which can be made from a InAs/AlSb T2SL (B_p), and an active layer (AL) made from a *p*-type InAs/GaSb T2SL (*p*). In Figure 1, "X" is replaced by "*n*" or "*p*" if the CL is made from the same material as the AL, and "C_n" or "C_p" if the CL is made from a different material to the AL (e.g. an *n*- or *p*-type InAs/AlSb T2SL). In all cases, the depletion region is excluded from the narrow band gap photon absorbing AL, and instead confined to the much wider band gap BL, so any G-R current from the narrow band gap AL is strongly suppressed. Exclusion is achieved by ensuring that the BL and AL are both doped *p*-type. It also creates the interesting situation of a completely unipolar pB_pp device which behaves in many ways like a photovoltaic detector with a gain of one, even though it contains no *p*-*n* junction[4].

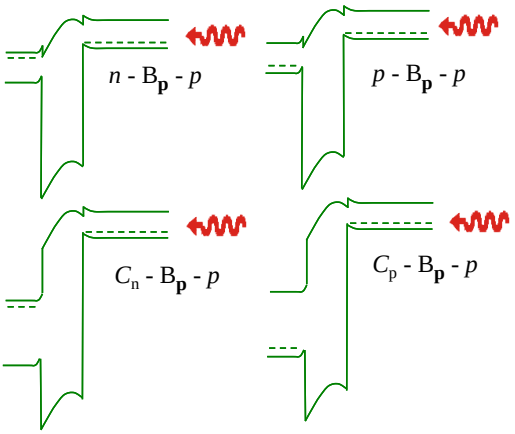

Figure 1
The four contact configurations of an $XB_p p$ detector.

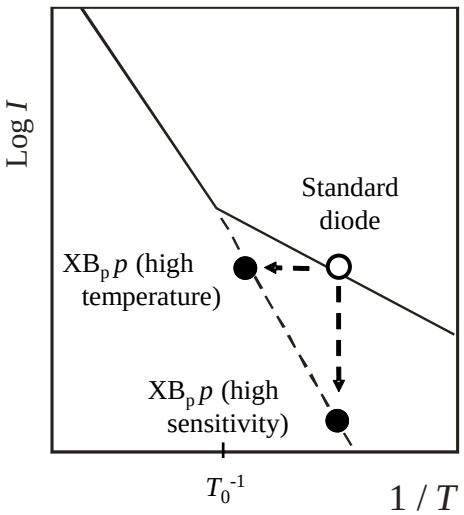

Figure 2
Schematic Arrhenius plot of the dark current in a Standard diode (solid line) and in an $XB_p p$ barrier device (dashed line). Solid circles show the operating points for the $XB_p p$ device with improved sensitivity or a higher operating temperature

Figure 2 shows a schematic Arrhenius plot of the dark current in a standard photo-diode, in which the G-R contribution has a lower slope than the diffusion contribution. This is because it is activated with approximately half the energy. The two contributions are equal at the crossover temperature T_0, which increases with the active layer (AL) band gap energy[5]. When the G-R current is suppressed in an $XB_p p$ detector, the device has a higher operating temperature than the equivalent photo-diode operating with the same dark current (see horizontal arrow in Figure 2). On the other hand the dark current of the $XB_p p$ detector is lower than that in the photo-diode when the two devices are operated at the same temperature. This makes the $XB_p p$ detector more sensitive than the photo-diode (see vertical arrow in Figure 2). The difference in dark current for two such devices is demonstrated experimentally in the next section.

3. DESIGN AND PERFORMANCE OF T2SL BARRIER DEVICES.

Figure 3 (a) shows a schematic band structure for the barrier layer and active layer of an XB*p* device based on InAs/GaSb and InAs/AlSb T2SLs, respectively. In (b) the edges of the mini-bands shown in (a) are sketched for an operating pB_pp device, where all layers are doped *p*-type. The advantage of the barrier device is demonstrated in Figure 4, which compares a standard LWIR *n*-on-*p* diode based solely on InAs/GaSb and operating at a bias of 0.1V, with a

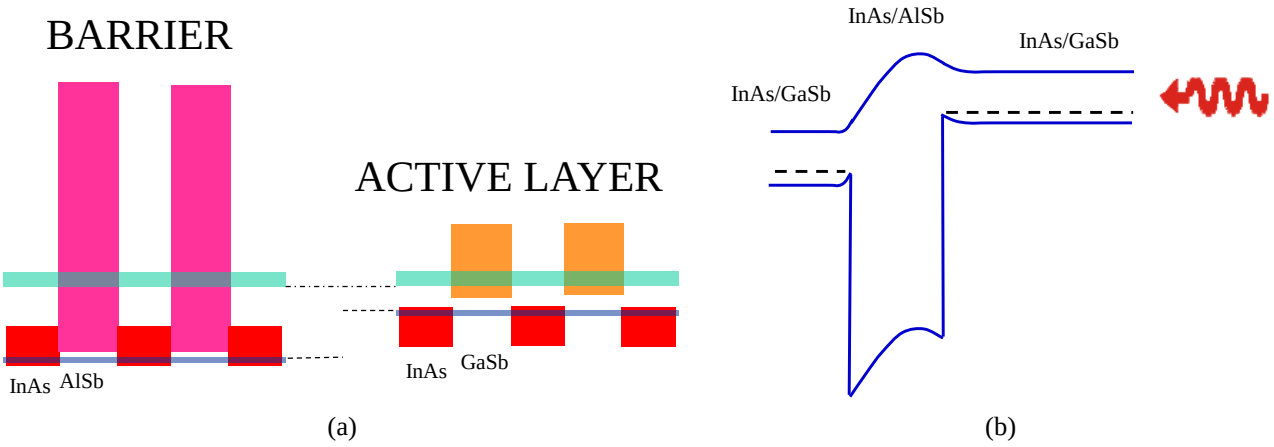

Figure 3
(a) Alignment between mini-bands in the active and barrier layers of a T2SL XB*p* device, super-imposed on the band gaps of InAs, GaSb and AlSb (b) Schematic profile of band edges in an operating pB_pp device, based on the mini-bands shown in (a)

LWIR pB_pp device based on the design in Figure 3, and operating at a bias of 0.6V. Both devices have an active layer band gap wavelength close to 10 μm. The barrier device (blue line) is diffusion limited down to 77K, while the diode (red line) is G-R limited at this temperature, with a dark current over 20× larger. The dark current in our pB_pp test devices is within one order of magnitude of MCT Rule-07, which is the performance standard for state of the art MCT photo-diodes[6].

It is now shown how we are able to simulate the full spectral response for an FPA made from the pB_pp device shown in Figure 3, if the thickness of the InAs and GaSb layers in the T2SL period are known. This allows us to design the superlattices inside the structure correctly, prior to MBE growth. The simulation is based on a **k · p** treatment and optical transfer matrix (OTM) calculation recently reported elsewhere[7]. While the OTM technique is fairly standard, the **k · p** treatment contains a number of innovations.[8] This treatment leads to a reduced number of fitting parameters compared to other approaches, namely two independent Luttinger parameters (of InAs), three interface parameters, the valence band offset and a parameter close to unity that is related to the interband momentum matrix element. The same two Luttinger parameters are used for all superlattices of the form InAs/X where X=GaSb or AlSb, so they only need to be determined once. The fitted values turn out to be very close to those determined by other workers.[8] All other parameters used in the calculation are based on established spectroscopic, mechanical or X-ray data available in the literature.

Figure 5 (a) compares the full absorption spectrum calculated with the **k · p** model (black line) for a 14.4/7.2 InAs/GaSb LWIR T2SL (dimensions in monolayers (ML)) with an experimental spectrum (grey line) for this T2SL. Both the absolute absorption coefficient and the main spectral features appear to be reproduced quite well, including the strong peak just above 2 μm. This peak is due to superlattice zone boundary transitions between HH_2 and E_1, and is discussed in detail in Ref. 8. It should be noted that the absorption edge of the T2SL is fairly broad unlike that for the MWIR T2SLs reported in Ref. 8. The reason for this is that a very low doped GaSb substrate was used to grow the LWIR T2SL, so that an absorption measurement could be performed up to a wavelength of 12 μm without the need to thin the substrate. In contrast doped substrates were used for the MWIR T2SLs because these are sufficiently transparent in the shorter wavelength range. The doped substrates had a higher crystalline quality and for this reason the MWIR T2SLs exhibit a much smaller inhomogeneous broadening[8]. The LWIR

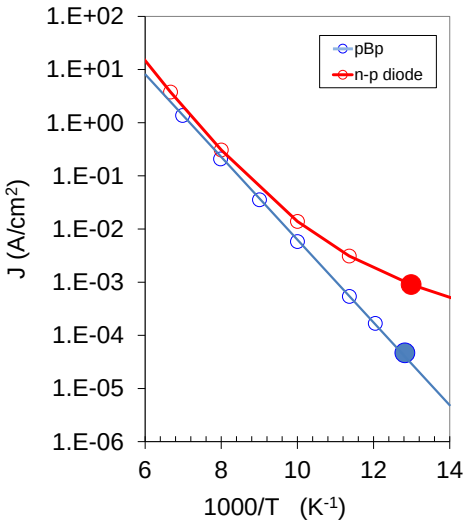

Figure 4
Log J_{dark} vs. 1000/T in pB_pp barrier device (bias = 0.6V) and *n-p* diode (bias = 0.1V), each with an InAs/GaSb active layer bandgap wavelength of λ_G ~ 10 μm (mesa area = 100×100 μm²)

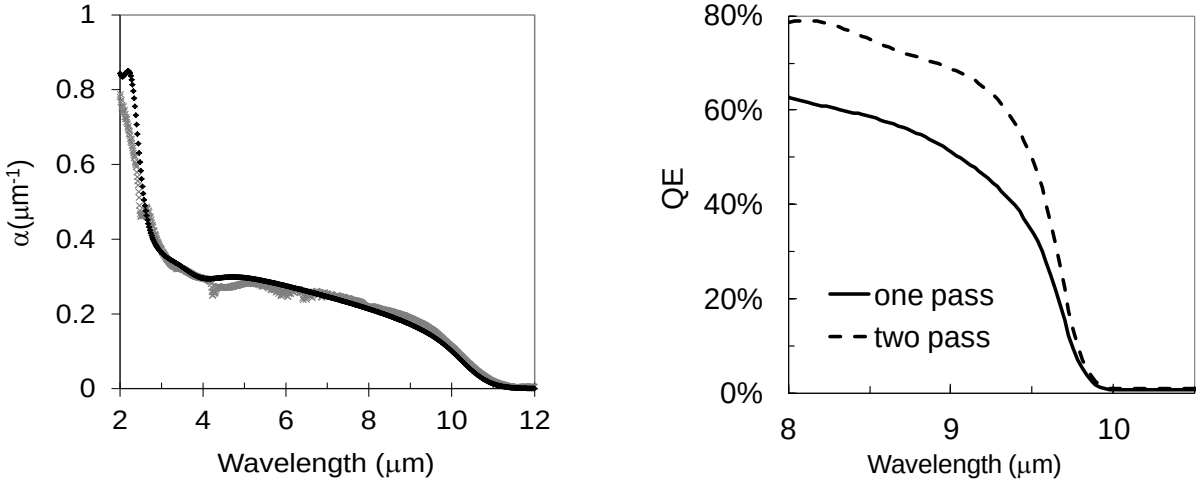

(a) (b)

Figure 5

(a) Measured (grey line) and calculated (black line) absorption spectra for a 14.4/7.2 InAs/GaSb T2SL (dimensions in ML) and (b) calculated spectral response for a $XB_p p$ detector with a 4.5 μm thick AL made from a 13.8/7 InAs/GaSb T2SL when none of the LWIR radiation (solid line) or 80% of the LWIR radiation (dashed line) is reflected back from the contact for a second pass through the AL.

T2SLs used to fabricate our $pB_p p$ detectors are also grown on doped substrates and these T2SLs have a more abrupt absorption edge, as for the MWIR T2SLs. Most of the doped substrate is removed later on in the fabrication process.

Figure 5 (b) shows an OTM calculation of the spectral response of a $pB_p p$ detector with an antireflection coating (ARC) and a 4.5 μm thick AL based on a 13.8/7 InAs/GaSb T2SL with a cut-off wavelength close to 10 μm. The OTM calculation uses a T2SL absorption spectrum deduced from the $\mathbf{k} \cdot \mathbf{p}$ model with narrow inhomogeneous broadening appropriate to growth on doped substrates. Although the InAs/AlSb BL makes no contribution to the detector response, the $\mathbf{k} \cdot \mathbf{p}$ treatment described above is also used to design the correct layer widths in the BL of the grown device. Figure 5 (b) shows curves for both a single pass device (solid line) and a two pass device (dashed line) in which 80% of the light impinging on the metal contact of the CL is reflected back for a second pass through the AL. It has been assumed that there are no losses of photo-carriers due to recombination in the bulk or at the surfaces (internal QE = 100%). Under these conditions, the two pass detector is able to provide an average QE of ~70%, defined as the spectral response in Figure 5 (b) weighted by the 300K black body radiation spectrum and averaged from the cut-on of the LWIR atmospheric widow (~8 μm) to the detector cut-off wavelength of 9.5 μm. The equivalent value for the single pass device is ~50% . We show below that the single pass value can be realized in a FPA which was designed as a one pass detector.

4. 640 × 512/15 μm DIGITAL ROIC

The new ROIC has an architecture that closely follows that of the mature and extremely successful MWIR Pelican D ROIC. This approach was chosen due to the excellent performance expected in terms of readout noise, Residual Non Uniformity (RNU), power dissipation and frame rate. Another important incentive was to support our incumbent customers with fast integration into systems and cameras. Nevertheless, the new T2SL LWIR technology poses two important challenges for the ROIC design:

1. The device polarity requires a polarity inversion in the ROIC circuitry.
2. The higher photon flux compared with the MWIR imposes very short integration periods due to the limited area available for the integration capacitors. To overcome this problem we have implemented a high frame rate (up to 360Hz) with frame averaging (up to 8 frames) performed in the proximity electronics. This enables us to achieve an NETD value @ F/2.7 and 30Hz of less than 15mK.

The ROIC was tested at room temperature and 77K and the results compared favorably with preliminary predictions. Table I presents the measured performance.

Parameter	Value
Well Capacity	> 6Me$^-$
Noise Floor	< 1300e$^-$
ROIC RNU	< 0.025% of DR
Dynamic Range	5350
ADC Resolution	13 bit (> 7000 DL)
Maximum Frame Rate	360Hz
Input Clock Frequency	80MHz
Power Consumption	110mW @ 360Hz
Operating Temperature	Functional at room temperature Full performance at 77K
Windowing	Supported
Up/Down Readout	Supported
Integration modes	ITR, IWR

Table I
Pelican-D LW ROIC performance

5. PELICAN-D LW FPA

"Pelican-D LW" is the first in our new line of LWIR XB$_p$*p* FPAs manufactured at SCD. The detector is based on a 15 µm pitch, 640 × 512 FPA bonded to the new digital silicon ROIC, described above. The FPA has a nominal cut-off wavelength of 9.5 µm. In the rest of this section, we present some of the key radiometric performance parameters of a Pelican-D LW FPA, measured in a laboratory test Dewar.

Figure 6 shows the FPA dark current distribution at 78K. The median value is close to 100 pA and the distribution is quite narrow with a full width at half maximum of only ~6% of the median value. It does not have a significant high current tail, and its narrow width demonstrates a high degree of uniformity. A narrow dark current distribution is very good for the stability of the FPA against temperature or bias fluctuations. The median dark current density is 4.4×10^{-5} A/cm^{-2}, which is within about one order of magnitude of the dark current range of MCT Rule-07[1].

The good uniformity of our T2SL FPA technology is well demonstrated in Figure 7, which shows a map of the raw signal registered (in digital levels) when the FPA is placed in front of a black body at 35°C before any non-uniformity correction has been performed. The map is very uniform, with no stains, large clusters or other variations across its area. This in turn lead to a very low RNU after a two point correction is performed. Figure 8 shows a plot of RNU vs. well fill (WF), measured using different black body temperatures and a constant integration time, with correction points at 54% and 72% WF, respectively. The RNU remains below 0.02% for WF values in the range 40 - 80%. Moreover, the FPA is very stable and can maintain a stable image for many hours without any further one or two point corrections.

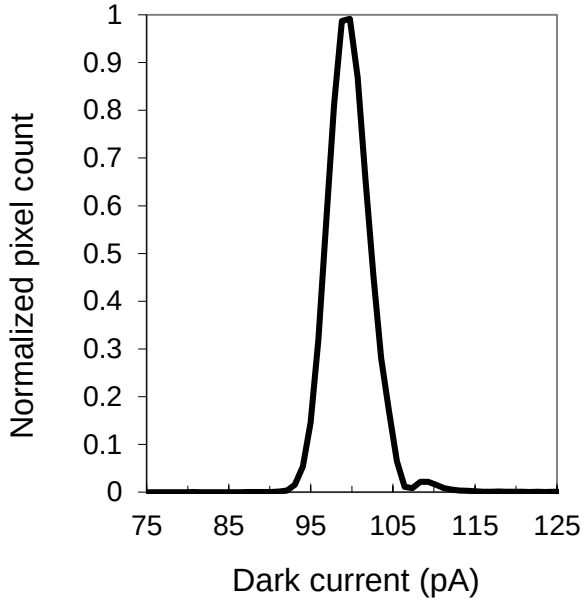

Figure 6
Dark current distribution of the Pelican-D LW FPA at 78 K

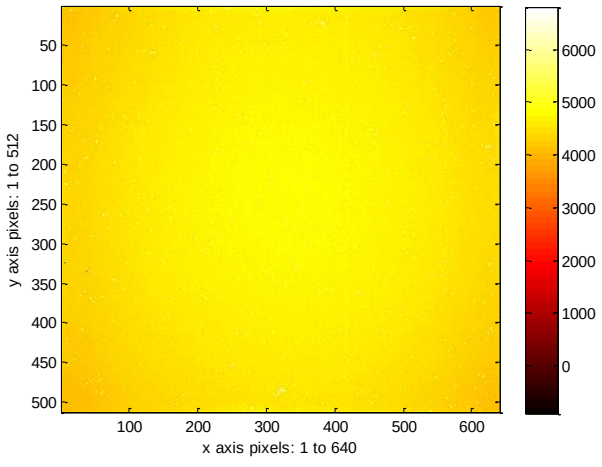

Figure 7
Raw signal map (in Digital levels) registered by the Pelican-D LW FPA, operating at 78K in front of a black body at 35° C.

At 65% well fill of its 6 Me capacitor and a frame rate of 240Hz, Pelican-D LW offers an NETD of 36 mK when configured with F/2.7 optics. By averaging 8 frames at a time, the detector operates at an effective frame rate of 30 Hz. The NETD distribution measured under these conditions is shown in Figure 9. It is narrow and symmetric with no pronounced tailing. The peak value is 13 mK which is a reduction of √8 relative to the single frame value. This is as expected for pure shot noise, and shows that any noise introduced by the averaging procedure is negligible.

In Figure 10 we show a map of the pixel QE in which none of the defective pixels have been removed. The total number of both hard and soft defects on the FPA, defined according to SCD's stringent production line criteria, is 1446 giving an FPA operability of 99.56% in this case.

In Figure 10, the QE values for each pixel are the average values over the usable LWIR spectral window, defined as the number of photoelectrons measured by the ROIC divided by the number of photons arriving at the detector after passing through a cold filter with a wavelength range of 7.6 - 9.5 μm and a flat transmission. For the measurement, the detector was placed in front of a black body with a temperature of 35°C. The QE map in Figure 10 shows an almost constant value of ~ 48% across the whole FPA, which agrees quite well with the value expected for a one pass detector with the same AL thickness (4.5 μm) discussed in the previous section. If we define the background limited performance (BLIP) temperature as the detector operating temperature at which the dark current is equal to the photocurrent, the QE and dark current results discussed in this section yield a BLIP temperature with F/2.7 optics of 90 K. This is significantly higher than the operating temperature of 77K. At 77K, the dark current is more than 15× smaller than the photocurrent and as noted above, its distribution is narrow, making for good image stability against small temperature fluctuations.

Finally, in Figure 11, we show an image registered with the Pelican-D LW FPA operating at 77K, and in Table II we show both the appearance of the IDCA itself, and a listing of its current performance specification.

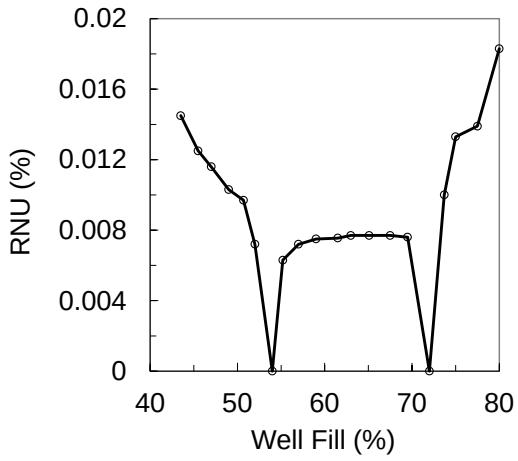

Figure 8
RNU of Pelican-D LW FPA at 78K after performing a two point correction at 54% and 72% well fill

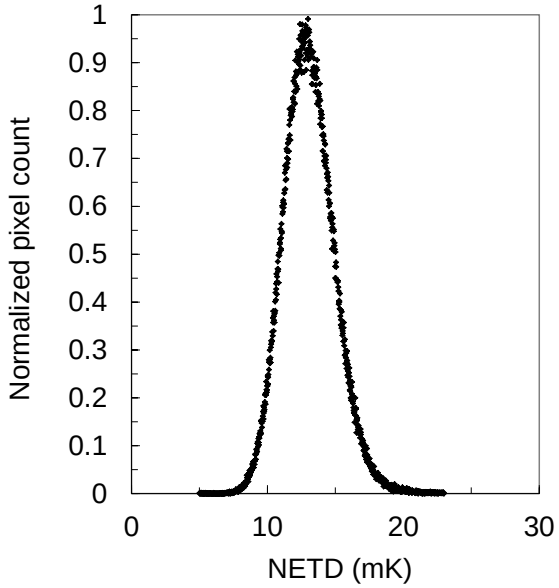

Figure 9
NETD distribution of the Pelican-D LW FPA at 78 K and at a frame rate of 30 Hz

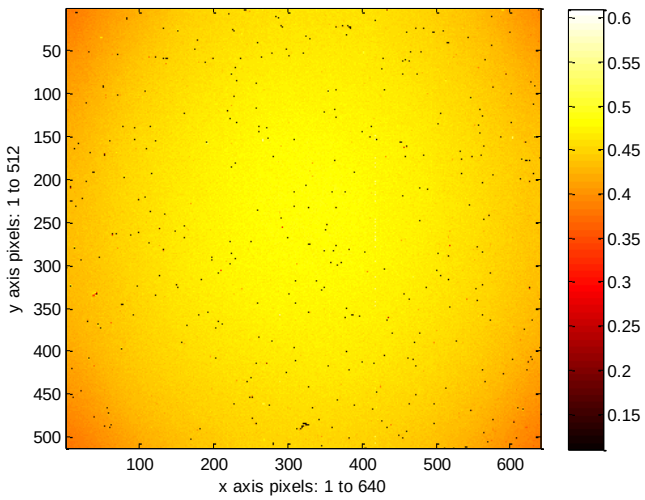

Figure 10
QE Map of the Pelican-D LW FPA operating at 78 K

Parameter	Value
Format	640 × 512
Pitch	15 μm
Cut-off wavelength	9.5 μm
Quantum efficiency	> 50%
Operability	> 99%
RNU	< 0.04% STD/DR @ 10 -90% Well Fill capacity
NETD	15mK @ 65% Well Fill capacity, 30Hz (by averaging 8 frames)
Response Uniformity	< 2.5% (STD/DR)
Electronics	Camera Link
Cooler	Ricor K548
Weight	750 gm
Environmental conditions	-40 to +71°C
Total Power at 23°C	16 W
Cool down time	8 min
MTTF (depends on mission profile)	15,000 hours

Table II
Image of Pelican-D LW IDCA and specification of performance at 77 K

6. CONCLUSIONS

In this article we have introduced Pelican-D LW, which is SCD's new LWIR FPA detector. It has a format of 640 × 512 with a 15 μm pitch, and operates at 77K with a nominal cut-off wavelength of 9.5 μm. The pixel operability is above 99%, according to SCD's standard production line criteria for the definition of bad pixels. The present version is a single pass detector with a QE of ~48% and exhibits very high uniformity and stability of its response and dark current. The FPA has an RNU below 0.02% of the dynamic range (DR) for well fills between 40 and 80% and a BLIP temperature at F/2.7 of 90 K. The active sensing material is based on a patented diffusion limited XB_pp barrier architecture, where an InAs/GaSb T2SL is used for the AL and an InAs/AlSb T2SL is used for the BL. We have shown that sophisticated simulation techniques exist at SCD which can predict the detector cut-off wavelength and spectral response a-priori, according to the individual layer thicknesses chosen for each superlattice period, and the overall active layer stack thickness. Pelican-D LW demonstrates the versatility of InAs/GaSb as a tunable active layer detector material, and shows that this material can now be considered to be a realistic alternative to MCT for small pitch, high performance LWIR FPA detectors.

Figure 11
Image registered with the 15 μm pitch, 640 × 512 Pelican-D LW FPA operating at 77K

ACKNOWLEDGEMENTS

The authors also acknowledge technical support from Mr. S. Greenberg, who was responsible for the smooth operation of the MBE machine, and Ms. H Schanzer, Ms. H. Moshe, Mr. Y. Caracenti, Ms. N. Hazan, Mr. I. Bogoslavski, Mr. Y. Osmo, Mr. M. Keinan, and Ms. M. Menahem who have all contributed to the successful processing, packaging or characterization of the devices.

REFERENCES

[1] W.E. Tennant, 2009 U.S. Workshop on the Physics & Chemistry of II-VI materials, Chicago, 2009

[2] A. Glozman, E. Harush, E. Jacobsohn, O. Klin, P.C. Klipstein, T. Markovitz, V. Nahum, E. Saguy, J. Oiknine-Schlesinger, I. Shtrichman, M. Yassen, B. Yofis, and E. Weiss, Proc. SPIE **6206**, 6206-0M, 2006

[3] P.C. Klipstein, *Depletionless Photodiode with Suppressed Dark Current*…, US Patent 7,795,640 (2 July 2003)

[4] P.C. Klipstein, *Unipolar semiconductor photodetector with Suppressed Dark Current*…, US Patent 8,004,012 (6 April 2006)

[5] P.C. Klipstein, *XBn Barrier Photodetectors for High Sensitivity and High Operating Temperature Infrared Sensors*, Proc. SPIE **6940**, 6940-2U, 2008

[6] P.C. Klipstein, E. Avnon, Y. Benny, R Fraenkel, , A. Glozman, S. Grossman, O. Klin, L. Langoff, Y. Livneh, I Lukomsky, M. Nitzani, L. Shkedy, I. Shtrichman, N. Snapi, A. Tuito and E. Weiss, Proc. SPIE **9070**, 9070-0U (2014)

[7] P.C. Klipstein, Y. Livneh, A. Glozman, S. Grossman, O. Klin, N. Snapi and E. Weiss, Journal of Electronic Materials, **43**, 2984 (2014)

[8] Y.Livneh, P.C. Klipstein, O. Klin, N. Snapi, S. Grossman, A. Glozman and E. Weiss, Phys. Rev. B **86**, 235311 (2012); Erratum, Phys. Rev. B **90**, 039903 (2014)